Partial Structure Functions of DNA Fragment Solutions. Concentration Effects

Leonore C. A. Groot, Maxim E. Kuil, Jaap C. Leyte, and Johan R. C. van der Maarel*

University of Leiden, Gorlaeus Laboratories, Department of Physical and Macromolecular Chemistry, P.O. Box 9502, 2300 RA, Leiden, The Netherlands

Jean-Pierre Cotton and Gerard Jannink

Laboratoire Léon Brillouin,† C.E. Saclay, 91191 Gif-sur-Yvette Cedex, France

Received: February 28, 1994; In Final Form: July 12, 1994⊗

The partial and charge structure functions of 163 base-pairs DNA fragment solutions are experimentally determined by small-angle neutron scattering at a relatively low concentration of 0.05 M nucleotides/L. In the momentum transfer range $q > 0.05$ Å^{-1}, the data agree with theoretical model calculations according to the cell model together with a distribution for the counterions around the rodlike DNA fragment obtained from the Poisson−Boltzmann equation. For $q > 0.075$ Å^{-1}, the scattered intensities agree with previous results on similar, but higher concentrated (i.e., 0.1 M nucleotides/L) solutions [van der Maarel; et al. *J. Phys. II (France)* **1992**, *2*, 109]. Unlike the previous data, the present results can be compared with the theoretical curves up to sufficiently low q values to check the theoretically expected low q upward curvature of the monomer−counterion and the counterion−counterion structure functions. A shell-like step radial counterion distribution as well as a model in which the condensed counterions are uniformly distributed within a cylindrical volume including the DNA molecule are checked and found to be in disagreement with the experimental data.

Introduction

The distribution of counterions about cylindrical polyelectrolytes has been studied using small-angle X-ray scattering.[1,2] In these experiments the relative contribution of the small ions was enhanced by using the heavy-metal counterions Cs^+ and Tl^+. The data were fitted to the relevant combination of the DNA, DNA−counterion, and counterion partial structure functions. The results agree with a radial counterion distribution profile calculated using the Poisson−Boltzmann equation in the cell model.[3−5] Small-angle neutron scattering is a useful method to investigate DNA solution structure. For instance, the spatial and orientational structure of DNA fragments in a cholesteric liquid crystal have been investigated.[6] Lederer et al. detected the solvation shell of 130 base-pairs DNA by solvent contrast variation in the presence of excess NaCl.[7]

By application of the solvent contrast method,[8] all partial structure functions of the dispersed particles can be unravelled. In particular, this kind of experiment has been performed on, e.g., charged micelles,[9] linear poly(styrenesulfonate)[10] and DNA fragment solutions.[11] In the latter work, aqueous DNA fragment (contour length $L = 500$ Å) solutions without added low molecular weight salt have been investigated at a concentration of 0.099 M nucleotides/L. These DNA fragments can be considered as rigid rodlike cylinders. The counterions were tetramethylammonium (TMA). In the present work, neutron-scattering results on similar but a factor of 2 less concentrated (i.e. 0.047 M) solutions are presented and compared to the former data. For the present DNA solutions, 74% of the counterions is TMA and the remaining 26% is sodium.

From the experimental scattering results, the nucleic acid monomer−monomer, the monomer−counterion, and the counterion−counterion partial structure functions are derived. The partial structure functions, obtained separately from the two data sets at different concentrations, are compared with theoretical model calculations. The theoretical curves have been derived using the cell model[3−5] and a counterion distribution around the rodlike DNA polyion obtained from the Poisson−Boltzmann equation. This model has two adjustable parameters, i.e., the polymer radius r_p and the distance of closest approach of the counterion to the DNA axis r_c. In the previous work,[11] these parameters have been determined by adjusting the theoretical structure functions to the experimental ones in the momentum transfer range $q > 0.075$ Å^{-1}. The same characteristic values agree with the present results.

Interference effects between different cell volumes, however, are not included in the model calculations. Due to these intercellular effects, the experimental data start to deviate from the theoretical curve below a certain q value. The range of momentum transfer q in which these interferences become significant depends on the concentration. This range shifts to lower q values with decreasing concentration. Accordingly, for lower concentrations, the cell model calculations are expected to agree with the experimental data in a more extended momentum transfer range.

For the 0.099 M DNA fragment solutions, interference effects become important for $q < 0.075$ Å^{-1}.[11] Therefore, similar measurements on DNA fragment solutions with a concentration as low as possible, considering reasonable counting times, appeared to be necessary. In the case of the present solutions, intercellular effects are of minor significance for $q > 0.05$ Å^{-1}. Here, the aforementioned partial structure functions coincide with the model calculations up to lower q values to confirm the calculated predictions of the model used to describe the counterion structure around the polyion.

Theory

In an aqueous DNA solution without added simple salt, the coherent part of the solvent subtracted scattered intensity reads[12]

* To whom correspondence should be addressed.
† Laboratoire commun CEA-CNRS.
⊗ Abstract published in *Advance ACS Abstracts,* September 1, 1994.

0022-3654/94/2098-10167$04.50/0

$$I(q) = c[\bar{b}_m^2 S_{mm}(q) + 2\bar{b}_m\bar{b}_c S_{mc}(q) + \bar{b}_c^2 S_{cc}(q)] \quad (1)$$

Here, c is the concentration in number of monomer nucleotides per unit volume and the monomer−monomer, monomer−counterion, and counterion−counterion partial structure function are denoted by S_{mm}, S_{mc}, and S_{cc}, respectively. For a H_2O/D_2O solvent mixture, the scattering length contrast $\bar{b}_i$ of the nucleotides (i = m) or counterions (i = c) is given by

$$\bar{b}_i = b_i - b_s\bar{v}_i/\bar{v}_s \quad \text{with} \quad b_s = Xb_{D_2O} + (1 - X)b_{H_2O} \quad (2)$$

Here, b_i and b_s are the scattering lengths of the dispersed particle and solvent, respectively. The corresponding partial molal volumes are denoted by $\bar{v}_i$ and $\bar{v}_s$. By variation of the D_2O mole fraction X, the scattering length contrasts $\bar{b}_i$ can be varied, and, hence, the partial structure functions can be determined. In the case of zero average contrast ($\bar{b}_m = -\bar{b}_c$) the scattered intensity is proportional to the charge structure function S_{zz}:

$$S_{zz}(q) = S_{mm}(q) - 2S_{mc}(q) + S_{cc}(q) \quad (3)$$

The structure functions can be theoretically calculated using the cell model[3−5] and the Poisson−Boltzmann equation. In this model the DNA fragment is represented by an uniform rod with length L and radius r_p, which occupies an electroneutral coaxial cell with radius r_{cell}. The cell radius is related to the concentration according to $cA\pi r_{cell}^2 = 1$. Here, A is the mean z-axis projected distance between nucleic acid monomers. Interference effects between different cell volumes are neglected.

In the longitudinal (z) direction, the distribution of the counterions is assumed to be uniform. The radial counterion distribution $\varrho_c(r)$ is obtained from the solution of the Poisson−Boltzmann equation for an uniformly charged cylinder with charge density $e/A\pi r_p^2$. The distance of closest approach of the counterion center of mass to the polymer z axis is denoted by r_c. Please note that r_c is not equal to r_p due to the finite counterion size and/or intermediate hydration water.

The values of the different geometric parameters are collected in Table 1. The polymer radius r_p and the distance of closest approach r_c were obtained from previous work on similar DNA fragment solutions, but at a concentration of 0.099 mol of P/L.[11] Due to the factor of 2 difference in concentration, in the present work the cell radius amounts 81.1 Å instead of 55.8 Å. Moreover, the DNA fragments are somewhat longer (L = 550 Å) than used previously (L = 500 Å) due to a different biochemical isolation procedure.

Under the neglect of interference effects between different cell volumes, the partial structure functions can be evaluated. For an extensive description of this evaluation, refer to the Appendix of ref 11. The result is given by

$$S_{ij}(q) = \frac{1}{N}\int_0^1 d\mu \left[\frac{\sin(q\mu L/2)}{(q\mu L/2)}\right]^2 P_i(q,\mu)\, P_j(q,\mu) \quad (4)$$

with $\mu = \cos\theta$, θ being the angle between the momentum vector $\boldsymbol{q}$ and the polymer z axis. For the step like radial monomer distribution, one has (i = m)

$$P_m(q,\mu) = 2N\frac{J_1(qr_p\sqrt{1-\mu^2})}{qr_p\sqrt{1-\mu^2}} \quad (5)$$

with N the number of nucleotides per DNA fragment ($=L/A$) and J_1 the first-order Bessel function of the first kind. For the radial counterion distribution $\varrho_c(r)$, as obtained from the solution of the Poisson−Boltzmann equation, the related $P_c(q,\mu)$ has to be evaluated by numerical integration of

$$P_c(q,\mu) = 2\pi L\int_0^{r_{cell}} dr\, rJ_0(qr\sqrt{1-\mu^2})\varrho_c(r) \quad (6)$$

Here, J_0 denotes the zero-order Bessel function of the first kind.

TABLE 1: Geometric Parameters Used for the Model Calculations in the Case of 0.047 M DNA Fragment Solutions[a]

L	550 Å
A	1.71 Å
ξ	4.18
r_{cell}	81.1 Å
r_p	8 Å
r_c	14 Å

[a] L represents the polymer fragment length, A the mean z axis projected distance between the nucleotides, and ξ the linear charge density parameter Q/A, with Q the Bjerrum length (for T = 278 K in water, Q = 7.14 Å). The cell radius is denoted by r_{cell} and the polymer radius by r_p, whereas r_c is the distance of closest approach for the counterions to the polymer rod axis.

Experimental Section

DNA fragments were obtained by a micrococcal nuclease digestion of calf thymus nucleosomal DNA, following the procedure described by Wang et al.[13] After precipitation in cold 2-propanol, the DNA pellet was dried under reduced pressure at room temperature. The DNA was brought to the salt free tetramethylammonium (TMA) form by dialysis with 0.1 M TMACl against pure water. To avoid denaturation, care was taken that the DNA concentration did not reach values below 3 mM nucleotides/L. Water was deionized and filtered by a Millipore water purification system (Millipore Co.), and its conductivity did not exceed 1×10^{-6} Ω^{-1} cm^{-1}. The final product was freeze-dried and stored at 255 K.

To determine the DNA fragment molecular weight distribution, gel permeation chromatography has been performed on sodium DNA fragments of the same preparation. Some low molecular weight material was present, but at least 75% of the DNA had a M_w/M_n ratio smaller than 1.1 and was characterized by a M_w of 108 000 (163 base-pairs). Atomic absorption spectroscopy experiments on the TMA form of the DNA fragments showed that the sodium ion content was still 26% after the dialysis procedure. For this material, the ratio of the optical absorbances A_{260}/A_{280} is 1.85, which indicates that it is essentially free of protein. The hyperchromic effect is about 30%, indicating that the DNA fragments were not denaturated during the dialysis procedure.

Four samples have been prepared by dissolving the material in four different H_2O/D_2O solvent compositions. The DNA concentration as well as the isotopic H_2O/D_2O composition of the samples have been determined by weight. To calculate the composition and the DNA concentration of the samples, the water content of both the DNA and the D_2O have been determined by IR spectroscopy. The DNA concentration amounts 0.047 M nucleotides/L, which corresponds to 2.85×10^{-5} nucleic acid monomers/Å^3. Four reference samples consisting of four different H_2O/D_2O mixtures at the same isotopic composition have also been prepared.

The partial molal volumes and the scattering lengths of the various components are collected in Table 2. The nucleotide scattering length contrast has been calculated using the values reported by Jacrot[8] and according to the calf thymus base composition A:G:C:T:5-methylcytosine = 0.28:0.22:0.21:0.28:0.01.[14] The effect of exchangeable hydrogen has been taken into account. The counterion parameters are both weighed

TABLE 2: Partial Molal Volumes ($\bar{\nu}_i$) and Scattering Lengths (b_i) of the Various Components[a]

	$\bar{\nu}_i$ (cm³/mol)	b_i (10^{-12} cm)
nucleotide	172	9.772 + 2.020X
counterion[b]	60.9	−0.568
H_2O	18.0	−0.168
D_2O	18.0	1.915

[a] X denotes the D_2O mole fraction (effect of exchangeable protons). [b] Calculated according to 26% sodium and 74% TMA.

TABLE 3: Scattering Length Contrasts of the Nucleotide Monomers ($\bar{b}_m$) and the Counterions ($\bar{b}_c$) for Samples with Different Isotopic Compositions[a]

	$\bar{b}_m$ (10^{-12} cm)	$\bar{b}_c$ (10^{-12} cm)	X
sample 1	11.38	0.00	0
sample 2	3.66	−3.04	0.432
sample 3	0.07	−4.45	0.633
sample 4	−6.43	−7.01	0.997

[a] X denotes the D_2O solvent mole fraction.

averages, according to the mole fractions of TMA and sodium present in the solution. The scattering length contrasts have been calculated using eq 2 and the parameters from Table 2 and are shown with the corresponding isotopic compositions in Table 3.

Neutron-scattering experiments were performed using the PACE small-angle neutron scattering spectrometer, situated on the cold source of the Orphée reactor at the Laboratoire Léon Brillouin, CEN Saclay. The incident beam wavelength was 6 Å. Two sets of data have been obtained in different configurations. In the first configuration, the effective distance between the sample and the detector was 1.50 m, allowing a momentum transfer of from 0.02−0.22 Å^{-1}. The counting time per sample, i.e., solution or solvent, was approximately 6 h. In the second configuration, the detector was placed at a distance of 1.15 m from the sample position. Here, the momentum transfer ranged from 0.03 to 0.28 Å^{-1} with a counting time of approximately 10 h/sample. Quartz cells with 0.1 or 0.2 cm (for D_2O containing samples) path length were used. The temperature at the sample position was controlled at 298 K.

Data correction allowed for the neutron wavelength dependence of the sample transmission and the detector efficiency. Scattering intensities were normalized by reference to the direct beam. The scattering of the corresponding solvent was subtracted, and an incoherent scattering correction has been performed (≈0.01 cm^{-1}).

Results and Discussion

The counterion scattering length contrast for sample 1 is approximately zero (see Table 3), so the measured intensity is directly proportional to the monomer−monomer partial structure function. For sample 3, the nucleotide scattering length contrast is close to zero. Here, the scattering data essentially represent the counterion−counterion partial structure function. In the case of sample 4, both scattering length contrast parameters have a sizeable value, resulting in a relatively intense scattering. For sample 2, $\bar{b}_m$ and $\bar{b}_c$ have values of the same order of magnitude, but opposite signs. Unfortunately, the zero average contrast condition is not exactly fulfilled, so the charge structure function is not directly measured. However, the data represent an overdetermined set from which the three partial structure functions can be derived, and hence the charge structure function will be constructed by combination according to eq 3. All four scattering curves are shown in Figure 1. For all samples, the data obtained in the two different configurations agree well in the overlapping q range 0.03−0.22 Å^{-1} (both data sets are displayed with the same symbol).

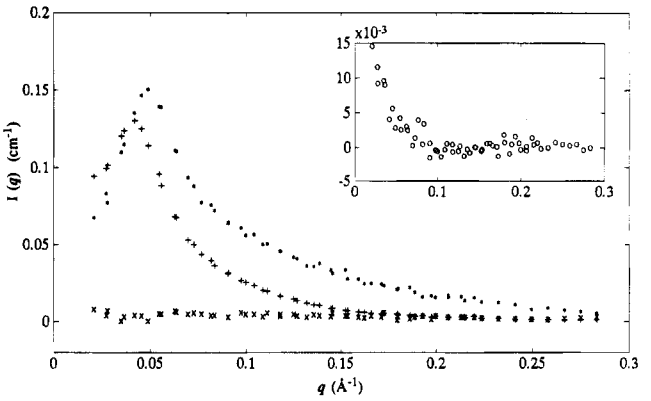

Figure 1. Corrected scattering intensity $I(q)$ vs momentum transfer q for sample 1 (*), sample 2 (×) and sample 4 (+). The D_2O mole fraction of these samples is 0, 0.432, and 0.997, respectively. The inset shows the corresponding data for sample 3 ($X = 0.633$) using the same units.

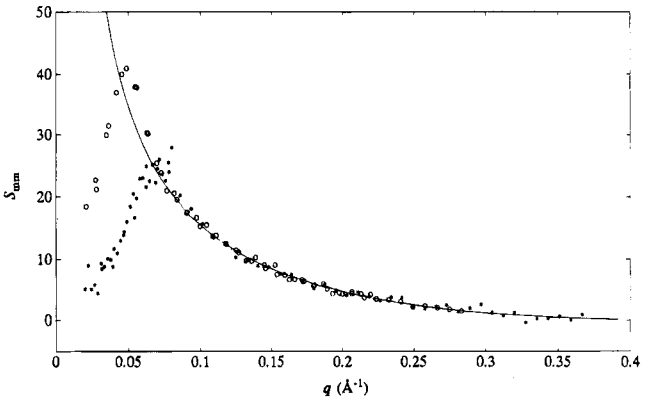

Figure 2. Monomer−monomer partial structure function S_{mm} for the 0.047 M (○) and the 0.099 M (*) solutions. The solid curve represents the form function of a uniform rod with $L = 550$ Å and $r_p = 8$ Å. For clearness' sake, the corresponding function for $L = 500$ Å is not included, since it coincides with the displayed form function for $q > 0.04$ Å^{-1}.

Using eq 1 together with the concentration and the contrast length parameters (see Table 3), the monomer−monomer partial structure function can be obtained from the scattered intensity from sample 1. As absolute intensity SANS measurements are notoriously difficult, an additional normalization was necessary. For this purpose, the scattered intensity from sample 1 was normalized to $c\bar{b}_m^2$ times the theoretical form function of a rod in the momentum transfer range $q > 0.075$ Å^{-1}. In this q range, any possible intercellular and/or intermolecular effects are negligible, as will be detailed below. This resulted in a multiplication factor of 0.74, which was subsequently applied to the scattering data of all samples. Afterwards, the three partial structure functions S_{mm}, S_{mc}, and S_{cc} have been obtained by orthogonal factorization in a least-squares sense.[15] The results are displayed in Figures 2−4, respectively. The corresponding data obtained earlier on 0.099 M DNA fragment solutions[11] have also been included.

In Figure 2 the nucleic acid monomer−monomer structure functions S_{mm}, experimentally determined for both concentrations, are shown. For $q > 0.075$ Å^{-1}, both data sets coincide. In the relevant q range, the theoretical form function is hardly affected by a small difference in polymer length ($L = 550$ Å for the present results vs $L = 500$ Å for the 0.099 M solutions). Accordingly, only the form function of a rod with $L = 550$ Å

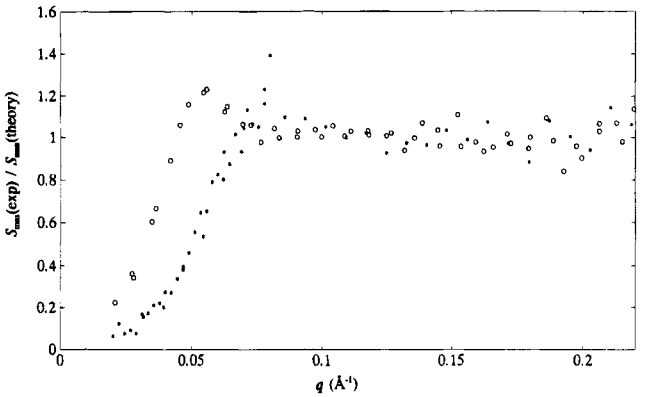

Figure 3. Intermolecular structure function for the 0.047 M (O) and the 0.099 M (*) solutions.

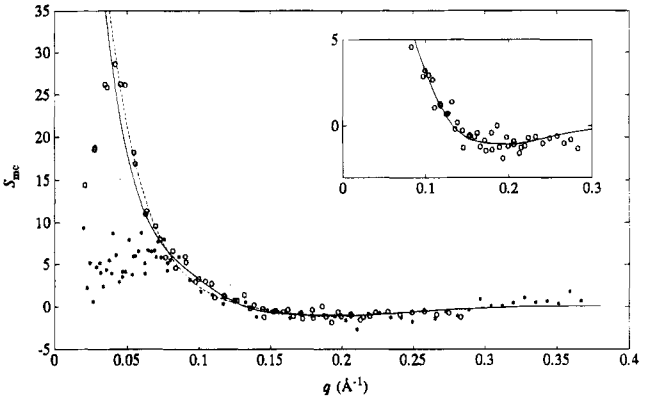

Figure 4. As in Figure 2, but for the monomer−counterion partial structure function S_{mc}. The solid curve represents the corresponding theoretical calculations with L = 550 Å, r_p = 8 Å, and r_c = 14 Å at a concentration of 0.047 M nucleotides/L. The theoretically calculated S_{mc} for the 0.099 M solutions (L = 500 Å, r_p = 8 Å, and r_c = 14 Å) is represented by the dashed curve. The inset shows a magnification in the case of the 0.047 M solutions for the q range in which the minimum occurs using the same units.

is displayed in Figure 2. In the calculation, a polymer radius r_p of 8 Å is used, as has been determined in the previous work.[11]

Intercellular and/or intermolecular effects are not included in the theoretical calculations. In the low q range, the corresponding contributions to the structure function become pronounced and the experimental data start to deviate from the theoretical curves. As the concentration is lowered, these interferences occur on a larger distance scale, and hence the corresponding scattering contributions shift to smaller q values. Consequently, the theoretical partial structure functions agree with the present experimental data in a somewhat more extended momentum transfer range.

To illustrate the intermolecular contribution to the monomer−monomer partial structure function, in our previous contribution the rod form function was subtracted from the experimental data.[11] Here, the experimental data are divided by the form function, a common procedure for systems with spherical symmetry. The result is displayed in Figure 3. For these highly charged polyions without excess salt, a closed analytical expression of this intermolecular structure function is not available. Weyerich et al. performed Monte Carlo simulations for charged rods modeling the tobacco mosaic virus.[16] They observed that with decreasing concentration, but above the overlap concentration c^* ($=L^{-3}$), the maximum in the intermolecular structure function becomes more pronounced and shifts to lower q values. The same qualitative behavior is observed for the DNA fragment solutions ($c \approx 15c^*$), as

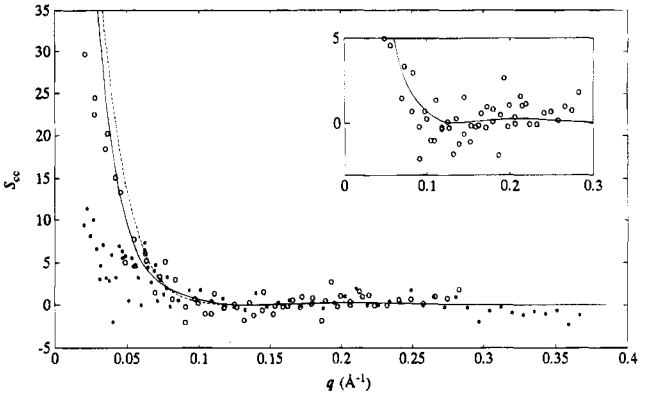

Figure 5. As in Figure 3, but for the counterion−counterion partial structure function S_{cc}. The inset shows a magnification in the case of the 0.047 M solutions for the q range in which the maximum occurs using the same units.

displayed in Figure 3. For the 0.099 M data, the maximum is not clearly resolved, but the intermolecular structure function starts to deviate significantly from unity for $q < 0.075$ Å^{-1}. In the case of the 0.047 M data, a weak maximum is observed at $q \approx 0.05$ Å^{-1}. As can be seen in Figure 2, for the latter data the agreement between the experimental data and the theoretical form function extends to $q \approx 0.05$ Å^{-1} and confirms the previously determined value for r_p.

As mentioned in the theoretical section, the structure functions S_{mc} and S_{cc} can be calculated using the Poisson−Boltzmann equation and cell model[3−5] together with the geometric parameters of Table 1 (eqs 4−6). These results for S_{mc} and S_{cc} are displayed in Figures 4 and 5, respectively, together with the corresponding experimental partial structure functions. Besides the aforementioned polymer radius r_p, the model calculations have a second adjustable parameter, i.e., the distance of closest approach of the counterions to the DNA axis r_c. In the previous work[11] this parameter was also optimized to adjust the calculated structure functions to the observed data. Since both the values for r_p and r_c are not expected to be affected by the concentration, they are also used in the present calculations. The Poisson−Boltzmann equation does not take into account small ion correlation effects. The function S_{cc} is solely based on the predicted radial counterion distribution function.

As has been observed before in Figure 2 for S_{mm}, the theoretical structure functions are hardly affected by the small difference in polymer length L. Moreover, in the relevant q range, the present concentration difference is of minor influence on S_{mc} and S_{cc}, as can be seen in Figures 4 and 5. For both S_{mc} and S_{cc}, the experimental data at the two different concentrations agree reasonably well in the momentum transfer range $q > 0.075$ Å^{-1}, as has also been observed for the monomer−monomer partial structure function (see Figure 2). In this q range, interference effects between different cell volumes are of minor importance for both concentrations. In the data reduction it is assumed that the distribution of the 26% sodium ions is similar to the distribution of TMA (mole fraction averaged contrast length parameters were applied). As displayed in Figures 4 and 5, this procedure leads to monomer−counterion and counterion−counterion partial structure functions, which are consistent with our previous results. Accordingly, a possible difference in sodium and TMA counterion distribution must have a minor influence on the present results.

In the case of 0.047 M DNA fragment solutions, the experimental data coincide well with the model calculations for $q > 0.05$ Å^{-1}, whereas the 0.099 M data deviate from the theoretical curves for $q < 0.075$ Å^{-1}. This small difference in

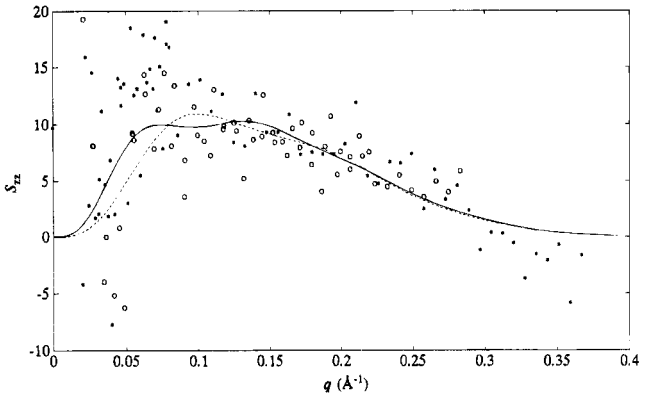

Figure 6. Charge structure function S_{zz} derived from the combination of the partial structure functions according to eq 3 for the 0.047 M (O) and the 0.099 M (*) solutions. The solid and the dashed curve represent the corresponding cell model calculations, respectively.

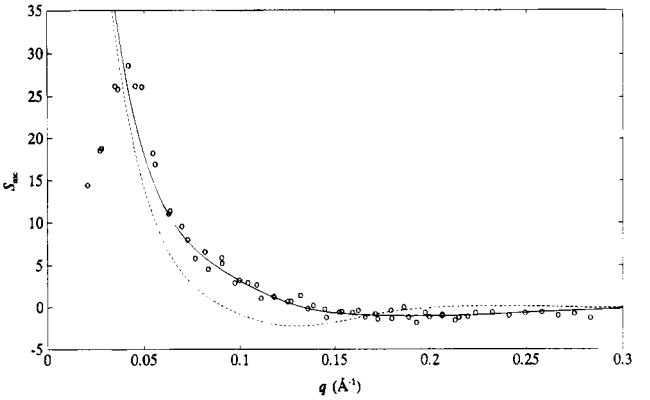

Figure 7. Monomer−counterion partial structure function S_{mc} for the 0.047 M (O) solutions together with the corresponding theoretical curves including the various radial counterion distribution profiles. The solid curve results from the counterion distribution obtained from the Poisson−Boltzmann equation. For the dashed curve, shell-like step model was used. The dotted curve corresponds to a profile in which the condensed counterions are uniformly distributed within a cylindrical volume including the DNA molecule.

q range is especially important to confirm the theoretically expected upward curvature of the structure functions S_{mc} and S_{cc} at low values of momentum transfer. For the higher concentrated solutions this upward curvature is to some extend obscured by interference effects, especially in the case of S_{cc}. The experimental data agree with the theoretical model calculations, whenever intercellular interferences are negligible. This confirms the suitability of the cell model including a counterion charge distribution obtained from the Poisson−Boltzmann equation. The upward curvature in S_{mc} and S_{cc} has also been observed in the case of the more flexible synthetic poly(styrenesulfonate) solutions.[10]

Due to the accumulation of counterions around the DNA molecule, the monomer−counterion structure function S_{mc} (see the inset in Figure 4) shows a broad, negative minimum. This minimum is sensitive to the value of r_c, i.e., the distance of closest approach of the counterion center of mass to the polymer axis. Within the accuracy of these measurements, there is no observable change in the position of the minimum by lowering the concentration. For both DNA data sets, this minimum occurs at $q \approx 0.2$ Å^{-1}, corresponding with $r_c = 14$ Å. For poly(styrenesulfonate), this minimum occurs at $q \approx 0.3$ Å^{-1}, in agreement with the difference in distance of closest approach r_c (9 vs 14 Å).[10] Unfortunately, the corresponding maximum in the counterion−counterion partial structure function (see the inset in Figure 5) is not clearly resolved due to the limited signal-to-noise ratio.

Figure 6 shows the charge structure function by taking the relevant combination of the experimentally obtained partial structure functions (see eq 3). The corresponding data on the 0.099 M solutions and the theoretical curves for both situations are included as well. As far as the theoretical curves are concerned, an oscillation shows up in the case of 0.047 M solutions. This is due to the charge separation at the polyion interface. The experimental data agree reasonably well with the model calculations, but the signal-to-noise ratio is too low to distinguish both maxima. Moreover, the limited signal-to-noise ratio does not allow detection of the concentration induced small differences in the charge structure function. Again, at low q values, the deviation from the theoretical curves is due to the neglect of long-range intercellular effects. Another neglected contribution is due to counterion fluctuations about the average concentration profile away from the polymer axis.[17]

In addition to the radial counterion distribution obtained from the Poisson−Boltzmann equation, two other radial distribution profiles have been checked. According to the condensation concept of Manning[18] and Oosawa,[19] a fraction of $1 - \xi^{-1}$ (ξ being the linear charge density parameter) of counterions are condensed. For the present DNA solutions, this fraction amounts 0.76. In the simple association model of Oosawa,[19] the radial counterion distribution corresponds to a steplike profile. The condensed counterion fraction is assumed to be uniformly distributed within a cylindrical shell with inner radius r_c (which is taken to be 14 Å) and outer radius r_{cond}. The remaining 24% are uniformly distributed within the coaxial shell with inner radius r_{cond} and outer radius r_{cell}. The value for r_{cond} is taken to be equal to the characteristic decay distance of radial counterion profile obtained from the Poisson−Boltzmann equation: $\chi^{-1} = 37$ Å. If the latter profile is integrated, the fraction 0.76 of the counterions is found to be within a radius of 41 Å away from the polymer axis. Since this value is not very different from χ^{-1}, the structure function calculations were performed using $r_{cond} = 37$ Å.

In the second model, the possibility for the counterions to occupy the grooves in the DNA molecule is included. For simplicity, it is assumed that the condensed counterions are uniformly distributed within a cylindrical volume with radius $r_c = 14$ Å. Outside this volume, the remaining counterion fraction is distributed according to the solution of the Poisson−Boltzmann equation, but with an effective linear charge density $\xi^{eff} = 1$.

Figure 7 shows the theoretical monomer-counterion partial structure function S_{mc} calculated with the various radial counterion distribution profiles. The corresponding data obtained on the 0.047 M DNA solutions are also included. It is clear that the profile obtained with the Poisson−Boltzmann equation agrees best with the experimental data. Both other models fail to describe the negative minimum at the relevant value of momentum transfer. The shell-like step model underestimates the local counterion concentration at relatively short distances of the order of r_c. This results in a shifting of the minimum to too low q values. The model in which the condensed counterions are uniformly distributed within a cylindrical volume including the DNA molecule, results in a S_{mc} which resembles the monomer−monomer partial structure function S_{mm}. For the counterion−counterion partial structure function S_{cc} and the charge structure function S_{zz}, the profile obtained from the Poisson−Boltzmann equation also describes the experimental data better in comparison with the other tested models (results not shown).

Conclusions

The present partial structure functions obtained from 0.047 M DNA fragment solutions agree with the corresponding data on similar 0.099 M solutions (obtained with the D17 diffractometer of the Institut Laue-Langevin, Grenoble) for $q > 0.075$ Å^{-1}. The model (i.e., the cell model in combination with the counterion distribution obtained from the Poisson−Boltzmann equation) and values of the adjustable parameters (i.e., $r_p = 8$ Å and $r_c = 14$ Å) agree with the present experimental data in the reciprocal space interval $q > 0.05$ Å^{-1}. In this interval interferences between different cell volumes are negligible. At lower q values these intercellular effects become important, and the experimental data start to deviate from the theoretical model calculations. This part of the data still needs to be interpreted. In contrast with the previous data, the present data can be compared with the theoretical curves up to sufficiently low q values to check the upward curvature in S_{mc} and S_{cc} characteristic for the model calculations.

The theoretical charge structure function agrees reasonably with the experimental data. However, the signal-to-noise ratio for this kind of low concentrated solutions is not sufficiently high to distinguish the predicted fine structure in the charge−charge partial structure function. Taking into account the rather extensive counting time per sample, measurements on similar solutions at even lower concentrations (i.e., below 0.047 M nucleotides/L) are not feasible yet.

Two alternative radial counterion distribution profiles were tested. A shell-like step model, which corresponds to Oosawa's association concept,[19] as well as a model in which the condensed counterions are uniformly distributed within a cylindrical volume including the DNA molecule do not agree with the experimental data. Other gradually decaying radial counterion distribution profiles, but with a similar distance of closest approach, cannot be excluded. This is due to the well-known problem of the inversion of scattering data to obtain the spatial density distribution.[20]

The present results are complementary to the results obtained by Chang et al.,[1,2] although they do not decompose their data into the partial structure functions. The counterion distribution obtained from the Poisson−Boltzmann equation agrees with their SAXS data, provided a considerable fraction of Cs^+ or Tl^+ counterions penetrates into the DNA grooves. Our neutron scattering data indicate the absence of significant penetration of TMA^+ counterions by the value of $r_c = 14$ Å. This might be related to a difference in cation radius between the heavy-metal ions and the TMA^+ ion used in the present study.

Acknowledgment. The authors acknowledge J. A. P. P. van Dijk for performing the gel permeation chromatography experiments, the staff of the Laboratoire Léon Brillouin for technical support, and M. Mandel for helpful discussions.

References and Notes

(1) Chang, S.-L.; Chen, S.-H.; Rill, R. L.; Lin, J. S. *J. Phys. Chem.* **1990**, *94*, 8025.
(2) Chang, S.-L.; Chen, S.-H.; Rill, R. L.; Lin, J. S. *Prog. Colloid Polym. Sci.* **1991**, *84*, 409.
(3) Alfrey, T. Jr.; Berg, P. W.; Morawetz, H. *J. Polym. Sci.* **1951**, *7*, 543.
(4) Katchalsky, A. *J. Pure Appl. Chem.* **1971**, *26*, 327.
(5) Mandel, M. *Encyclopedia of polymer science and engineering*, 2nd ed.; John Wiley & Sons Inc.: New York, 1988; part 11, p 739.
(6) Groot, L. C. A.; Kuil, M. E.; Leyte, J. C.; van der Maarel, J. R. C.; Heenan, R. K.; King, S. M.; Jannink, G. *Liquid Cryst.* **1994**, *17*, 263.
(7) Lederer, H.; May, R. P.; Kjems, J. K.; Baer, G.; Heumann, H. *Eur. J. Biochem.* **1986**, *161*, 191.
(8) Jacrot, B. *Rep. Prog. Phys.* **1976**, *39*, 911.
(9) Derian, P. J.; Belloni, L.; Drifford, M. *Europhys. Lett.* **1988**, *7*, 243.
(10) van der Maarel, J. R. C.; Groot, L. C. A.; Hollander, J. G.; Jesse, W.; Kuil, M. E.; Leyte, J. C.; Leyte-Zuiderweg, L. H.; Mandel, M.; Cotton, J. P.; Jannink, G.; Lapp, A.; Farago, B. *Macromolecules* **1993**, *26*, 7295.
(11) van der Maarel, J. R. C.; Groot, L. C. A.; Mandel, M.; Jesse, W.; Jannink, G.; Rodriguez, V. *J. Phys. II (France)* **1992**, *2*, 109.
(12) Jannink, G.; van der Maarel, J. R. C. *Biophys. Chem.* **1991**, *41*, 15.
(13) Wang, L.; Ferrari, M.; Bloomfield, V. A. *BioTechniques* **1990**, *9*, 24.
(14) Mahler, H. R.; Cordes, E. H. *Biological Chemistry*, 2nd ed.; Harper and Row: New York, 1971; Chapter 5.
(15) Matlab Numeric Computation Software; The Math Works Inc., 1991.
(16) Weyerich, B.; D' Aguanno, B.; Canessa, E.; Klein, R. *Faraday Discuss. Chem. Soc.* **1990**, *90*, 245.
(17) van der Maarel, J. R. C.; Mandel, M.; Jannink, G. *Europhys. Lett.* **1992**, *20*, 607.
(18) Manning, G. S. *J. Chem. Phys.* **1969**, *51*, 924.
(19) Oosawa, F. *Polyelectrolytes*; Dekker: New York, 1971.
(20) Duh, D.-M.; Haymet, A. D. J. *J. Phys. Chem.* **1994**, *100*, 2244.